Pure Appl. Geophys. 177 (2020), 4971–4982

https://doi.org/10.1007/s00024-020-02539-4

Pure and Applied Geophysics

Substorm Manifestations at Radio Paths of Oblique Ionospheric Sounding in the Arctic

D. V. Blagoveshchensky[1] and M. A. Sergeeva[2,3]

Abstract—The impact of geomagnetic substorms on radio propagation within the high-frequency (HF) range was analyzed using oblique ionospheric sounding data. These data were obtained from the unique system of radio paths that covers the whole region of the Russian Arctic. The study focused on the effects of two substorms with a twofold difference in intensity. Variations of four radio propagation parameters were studied: the maximum and lowest observed frequencies of the F2 ionospheric layer (F2MOF and F2LOF), and the same frequencies of the sporadic Es layer (EsMOF and EsLOF). Even the weak geomagnetic substorm ($AE_{max} \sim 500$ nT) significantly changed the ionosphere state and, consequently, the character of radio propagation at paths. The absorption of signals was more pronounced during a more intense substorm which resulted in loss of information during the transmissions through HF channels. The variations of propagation parameters (ΔMOF and ΔLOF) depend more on the path reflection point location and on the intensity of a substorm. Two substorms with a twofold difference in intensity had similar effects on ΔMOF, except for (a) the more pronounced smoothing of the Main Effect and (b) the higher ΔEsMOF amplitude during the intense substorm. Both issues are explained by more intense particle precipitations during the more intense disturbance.

Keywords: Geomagnetic substorm, ionosphere, oblique sounding, radio propagation, high-latitudes.

1. Introduction

Nowadays, exploration of natural resources in the Arctic region (for instance, in Canada, the USA, Norway, Russia) is one of the topical issues. A special focus is on the Arctic shelf, where oil and gas recovery is expected on a large scale. This implies the utilization of manpower resources under severe environmental conditions. People work in mining parties and production platforms, keep possible ship journeys, aviation and helicopter flights in the Arctic region. All these activities require reliable radio communication for all production sectors and users in the region. Satellite communications are reliable, but rather expensive. Another option is high-frequency (HF) communications, whose cost is relatively low. At the same time, it is susceptible to geomagnetic disturbances that are known to be most prominent at high latitudes (Hunsucker and Hargreaves 2003). There are numerous fruitful attempts to improve the quality of HF radio communication with the use of modern technology, for instance (Witvliet and Alsina-Pagès 2017 and references therein).

In addition, scientific research efforts have been focused on the problem of changes in the high-latitude ionosphere. Different aspects of these changes (case studies of disturbances, model assessments, absorption studies, etc.) were addressed in a number of works (Sreeja and Aquino 2014; Rogers and Honary 2015; Themens et al. 2017; Durgonics et al. 2017; Maltseva and Mozhaeva 2017; Kotova et al. 2015, 2020). It should be noted, HF ionospheric propagation is a significant issue for the International Telecommunication Union (ITU), especially at high latitudes, where predictions are difficult to make. There have been attempts to improve the understanding of the matter. For example, Athiento and Jayachandran (2016) discussed the discrepancies between maximum usable frequency (MUF(3000)F2) decile factors obtained from data in the Arctic region with the International Telecommunication Union (ITU-R) estimates. There are works dedicated to the peculiarities of the effects in high-latitude radio

[1] Saint-Petersburg State University of Aerospace Instrumentation, 67, Bolshaya Morskaya, Saint-Petersburg 190000, Russia.

[2] SCiESMEX, LANCE, Instituto de Geofisica, Unidad Michoacan, Universidad Nacional Autonoma de Mexico, Antigua carretera a Patzcuaro 8701, Morelia, Michoacan C.P. 58089, Mexico. E-mail: maria.a.sergeeva@gmail.com

[3] CONACYT, Instituto de Geofisica, Unidad Michoacan, Universidad Nacional Autonoma de Mexico, Antigua carretera a Patzcuaro 8701, Morelia, Michoacan C.P. 58089, Mexico.

channels (Siddle et al. 2013; Uryadov et al. 2012, 2017; Kotova et al. 2017; Blagoveshchenskii 2016; Ritchie and Honary 2009; Angling et al. 1997). Some of these works discussed in particular the substorm effects on the ionosphere, and less often on radio propagation at high latitudes. To give examples, Parkinson et al. (2004) took up the subject of substorm effects on variations in the behavior of SuperDARN Doppler spectral widths. Clilverd et al. (2008) studied the effects of substorm electron precipitation fluxes on low-frequency radio wave propagation conditions. The issues of HF propagation at high latitudes during substorms were also raised in Blagoveshchensky et al. (2005, 2009) and Milan et al. (1994, 1996). Changes in the HF propagation mechanisms caused by substorms were reviewed in Blagoveshchenskii (2013).

Nonetheless, the issue is still far from being fully resolved and needs further development. The aim of the current work was to analyze the substorm intensity impact on the HF signal propagation under otherwise similar conditions in the Arctic region. For this purpose, two substorms close in time and different by their intensities were chosen. The tasks were (a) to compare their influence on radio signal reflections from the ionosphere and (b) to reveal specific features of such impacts. Oblique ionospheric sounding (OIS) data obtained from the unique system of HF radio paths was used in the analysis.

2. Data Used

The OIS radio paths are operated by the Arctic and Antarctic Research Institute, Russia (www.aari.ru). The system of these paths is unique; there is no other such experimental OIS base in the world. The coordinates of the OIS stations are given in Table 1, and the station codes provided in the table are used throughout the text. Figure 1 shows the scheme of paths. The transceivers are mostly located along the coast of the Arctic zone in Russia. During night hours under quiet geomagnetic conditions, the majority of the considered paths are found in the southern part of the auroral zone and the circular area corresponding to maximal absorption (Fritz zone). It should be noted that during geomagnetic perturbations (for example, substorms), these zones are usually shifted towards the equator (Karpachev 2019).

Table 1

Coordinates of the stations whose data was used in the study

Site name/ city	Code	Lat. °N (geogr)	Lon. °E (geogr)	Lat. °N (geomag)	Lon. °E (geomag)
Amderma	AMD	69.47	61.42	68.85	147.62
Dikson	DIK	73.543	80.562	64.52	162.74
Lovozero	LOZ	67.97	35.02	63.37	126.76
Gorkovskaya	GRK	60.27	29.38	56.86	117.01
Salekhard	SAH	66.52	66.67	58.51	150.13
Sodankylä	SOD	67.367	26.633	63.98	119.53

The distances between the OIS transceivers are given in Table 2. In general, the lengths of the paths do not exceed 2000 km (except for the path DIK-GRK). This allows it to receive the OIS signals of one-hop mode propagation with reflections from both ionospheric regular F2 and sporadic Es layers. Transmission and reception of radio signals are provided by a specially designed equipment that operates in an automatic mode. Signals are emitted every 15 min during all hours. To avoid interfering signals at different paths, they are emitted with a time difference of several minutes in each radio channel.

Figure 2 provides examples of OIS ionograms taken at LOZ-DIK (upper panels) and GRK-AMD (lower panels) paths. The ionograms illustrated in panels (a) and (c) were taken during quiet geomagnetic conditions, and the ionograms in panels (b) and (d) during disturbance. The diffusivity of signals reflected from the F2-layer and the presence of the intense sporadic Es layers can be seen under disturbed conditions near midnight. There are no such effects under quiet conditions: the reflection occurred only from the F2-layer of the ionosphere. The ionograms in Fig. 2 are discussed in detail further in the text (Sect. 4.1). The analysis of the ionograms was focused on two main parameters of radio propagation: Maximum Observed Frequency (MOF) and Lowest Observed Frequency (LOF) reflected from both F2 and Es layers. Thus, four parameters were under analysis during substorms: F2MOF, F2LOF, EsMOF, EsLOF.

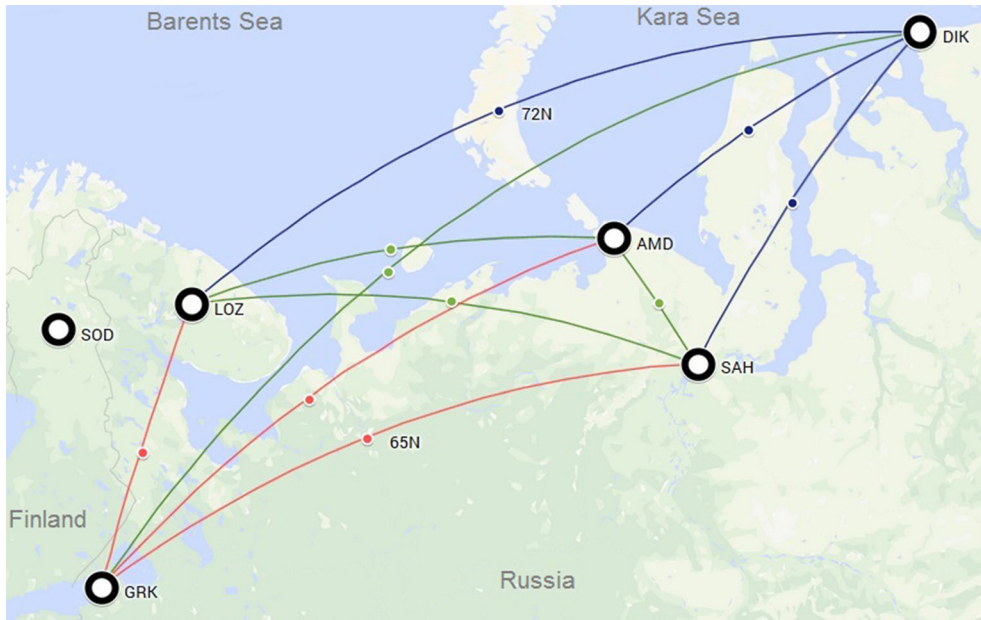

Figure 1
Map of OIS stations locations (black circles) and oblique sounding paths (lines between them) and mid-points of the paths (points). Three groups of paths are shown by three different colors

Table 2

Lengths of the HF paths in kilometers

Station code	GRK	LOZ	AMD	SAH	DIK
GRK	–	901	1754	1947	2555
LOZ	901	–	1020	1355	1730
AMD	1754	1020	–	435	836
SAH	1947	1355	435	–	938
DIK	2555	1730	836	938	–

3. Description of Substorms

Two substorms were chosen for the analysis. They were very close in time (days between them), which means the same solar cycle and season conditions as well as the absence of monthly variation effect which could affect the comparison of the ionospheric parameters during the two events. In addition, both substorms occurred in the near-midnight sector, with the beginning at 22:00 UT (Fig. 3). The first substorm occurred on February 7–8, 2014, and had a duration of 3.5 h. The second substorm occurred on February 15–16, 2014, and had a duration of 4.5 h. The durations of the substorms were defined by their explosive phases. The beginning of this phase is marked as T_o (onset) and its end as T_e (end). To reveal the changes in the ionosphere and the character of propagation during the considered substorms, the non-disturbed period of February 13–14, 2014, was chosen as a quiet background for comparison.

Figure 3 illustrates variations of the *X*-component of the magnetic field measured at SOD, the AE-index as a measure of global geomagnetic activity at high latitudes, and the absorption level A measured at SOD for both substorms. SOD was chosen as the station closest to the path system that had both magnetometer and riometer data. According to Fig. 3, the first substorm (panel a) was characterized by the maximal AE-index value of about 500 nT, with the maximal *X*-component deviation from its pre-substorm level of about 380 nT and with the maximal absorption level by riometer of about 1.8 dB. The second substorm (Fig. 3, panel b) was more intense. The maximal *X*-component deviation was about 830 nT, AE reached the value of 1052 nT, and the absorption level was 2.3 dB. Both events can be classified as moderate substorms. The second

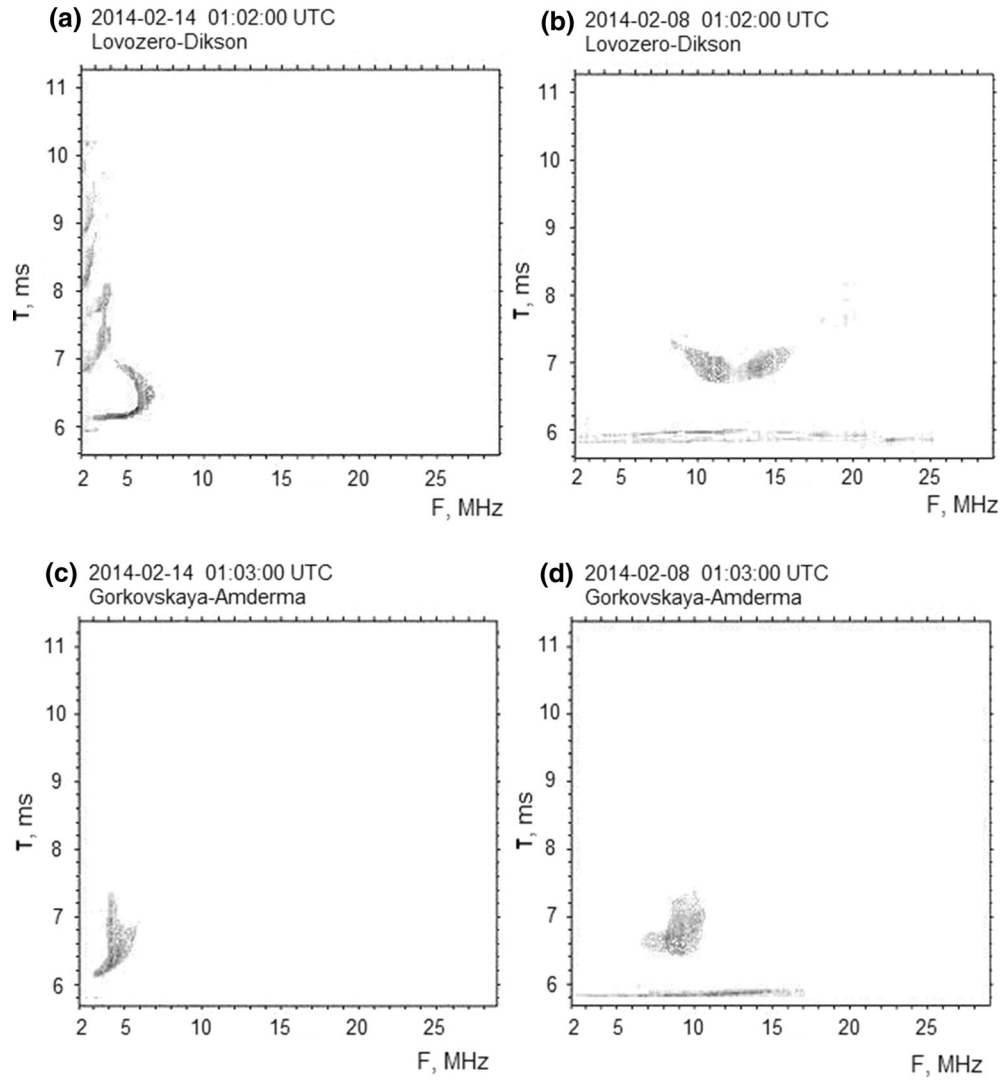

Figure 2
Ionograms taken at paths LOZ-DIK (**a**, **b**) and GRK-AMD (**c**, **d**). *F* is frequency

substorm was approximately twice as intense as the first substorm. Furthermore, significant variations of parameters (Fig. 3) were detected during the period between T_o and T_e: (22:00–01:30) UT for the first substorm and (22:00–02:30) UT for the second substorm. The substorms were chosen with different intensities but similar in other characteristics in order to study how the intensity of a substorm can affect the character of signal propagation at the OIS paths.

4. Discussion of Results

4.1. Characteristics of Signal Reflections

Figure 2 illustrates the ionograms for two paths: LOZ-DIK (upper panels) and GRK-AMD (lower panels). These paths have similar lengths (1730 km and 1754 km). They are almost in parallel to each other and extend approximately along the latitudes (Fig. 1, Table 1). LOZ-DIK is the more northern path. Its reflection point is located in the auroral oval.

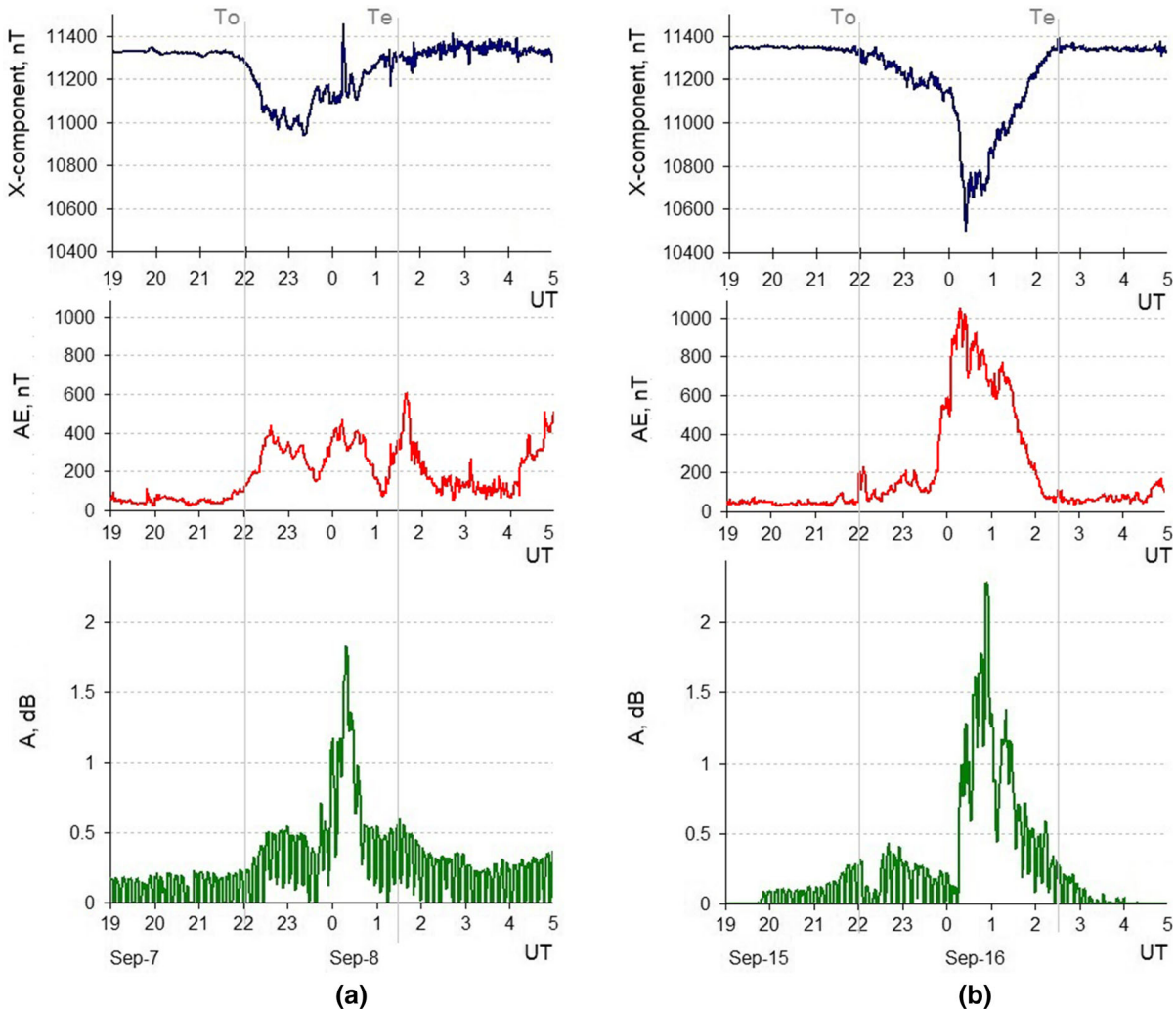

Figure 3
Variations of the *X*-component of the magnetic field (upper plots), AE-index (middle plots) and the absorption level (lower plots) before, during and after the explosive phases of the substorms occurred on February 7–8, 2014, (**a**) and February 15–16, 2014 (**b**)

The reflection point of GRK-AMD is at the southern edge of the oval.

We compared the ionograms obtained at 01:02 UT and at 01:03 UT on February 14, 2014 (under quiet geomagnetic conditions) with the ionograms taken at the same moments under disturbed conditions during the substorm on February, 8, 2014 (the weaker substorm of the two). It is worth noting that F2MOF values at near-midnight hours under quiet conditions are very low. The intense one-hop and two-hop reflections took place at the LOZ-DIK path under quiet conditions (Fig. 2a). Here, F2MOF = 7 MHz. Significant diffusiveness of signal reflections from the sporadic Es layer was observed at the same path during the disturbance (Fig. 2b). Here, F2MOF = 16 MHz, EsMOF = 25.3 MHz. Multiple-hop reflections were absent. The general picture of reflections is very different from that of the quiet period. There was only one reflection from the F2-layer with F2MOF = 6 MHz in the ionogram for GRK-AMD during the quiet period (Fig. 2c). The signal itself was rather dispersed. The last circumstance is most likely explained by the fact that the path's reflection point is located in the zone of

ionospheric irregularities concentrated in the southern part of the auroral oval. Figure 2, panel d, shows the diffuse reflection from the F2-layer with F2MOF = 11 MHz and the presence of Es-reflections with EsMOF = 17 MHz during the substorm.

The following can be concluded. First, MOF values of the more northern path are higher than at the more southern path in both quiet and disturbed periods. From a physical perspective, this is explained by the higher ionization rate in the center of the oval than at its edges. Second, even the weak storm significantly changes the ionospheric parameters and the character of radio propagation at the paths. The impact was more pronounced at the more northern path, which also could be expected as the influence of geomagnetic substorms generally decreases with latitude (towards the equator) (Hunsucker and Hargreaves 2003).

4.2. *Ionospheric Parameters Variations*

Figure 4 illustrates an example of MOF and LOF variations during the weaker substorm (February 7–8) (a), during quiet conditions (February 13–14) (b), and during the intense substorm (February 15–16) (c) at the SAH-GRK path, with a length of 1947 km. There were 10 such plots in total (for different OIS paths). Figure 4 shows the results for the most southern path from the path system shown in Fig. 1. Thus, it was chosen assuming the weakest impact of the substorm on it compared to more northern paths. All three plots in Fig. 4 show the same F2MOF feature: the decrease between 15 and 19 UT. The F2MOF minimum under quiet conditions took place near midnight.

Let us consider the disturbed conditions.

4.2.1 *The Weaker Substorm*

The upper panel in Fig. 4 shows the F2MOF increase beginning from 19 UT, which is 3 h before the substorm onset (T_o), probably because of the high-speed solar particles penetrating the ionosphere. Then, F2MOF decrease during the substorm is seen, which was followed by some decrease near the substorm end (T_e) and after it. This looks like a Main Effect (ME) in the ionosphere (Blagoveshchensky 2012; Danilov and Konstantinova 2019b). We recall briefly that the ME is a characteristic pattern of critical frequencies behavior, which is a sequence of the following critical frequency variations: (1) foF2 increase from its quiet median about 4-5 h before the substorm expansion phase; (2) foF2 decrease lower than its median just after T_o during the expansion phase; (3) the issue "1" phenomena general recurrence during the recovery phase and (4) two bell-shape foEs spikes about 3 h before T_o and during the expansion phase (within T_o-T_e). ME was discussed in detail in Blagoveshchenskii (2013), Blagoveshchensky et al. (2017) and Danilov and Konstantinova (2019a, b). The reader is referred to these works and references therein. To illustrate the effect, Fig. 5 shows the plot taken from Blagoveshchensky et al. (2017) (Fig. 1 in that work). It is a schematic representation of averaged ionospheric parameters ΔfoF2 and ΔfoEs variations during an averaged substorm. Δ is the parameter deviation from the median value of the undisturbed period. foF2 and foEs are the critical frequencies of the F2 and Es layers. The averaging before, during and after 72 substorms (mostly night substorms) in winter and equinoxes within the period 1993–1999 with a duration of 2–3 h was performed by epoch folding method. The data used in the analysis were from ionosonde stations located between 40 and 70 geomagnetic latitudes in Europe, Central Siberia and North America. The character of variations in Fig. 5 is qualitative because the stations are located at different coordinates and have different technical characteristics. F2MOF variations during the considered weaker substorm corresponded to the ME pattern.

Regarding Fig. 4, the F2LOF growth within T_o-T_e (22–01:30 UT) was due to the increased absorption (Fig. 3), as it is known that LOF depends on the increased absorption at a path. Es layers appeared with the substorm beginning (in accord with Fig. 5) and disappeared after its end. EsMOF values were significantly lower than F2MOF during the explosive substorm phase. EsLOF grew during the substorm and were probably controlled by the increased absorption.

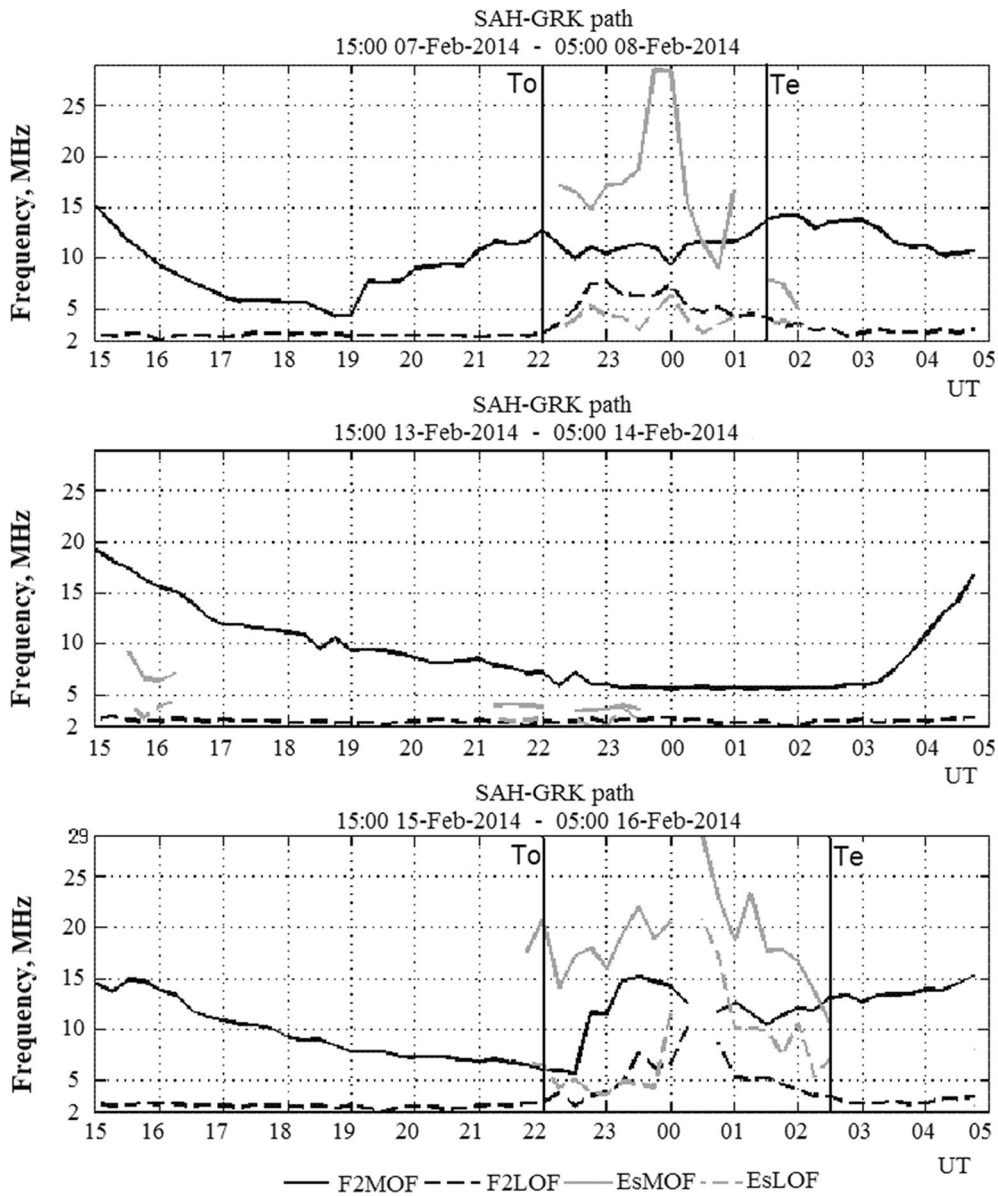

Figure 4
Variations of MOF and LOF by two layers during the weaker substorm (upper panel), quiet period (middle panel) and the more intense substorm (lower panel)

4.2.2 The More Intense Substorm

The lower panel in Fig. 4 shows the following dynamics. F2MOF values drastically increased at the substorm beginning at 22 UT, and then some decrease was observed, after which the growth was seen again near the end of the substorm at 02:30 UT. Here, the Main Effect in the ionosphere (Fig. 5) is also observed but with some shift in time (with delay). It should be noted the reflection point of the considered path is in the auroral oval during substorms. Therefore, although the Main Effect was present, it was covered with the dominating ionization caused by the auroral zone fluxes, as mentioned in issue 1.

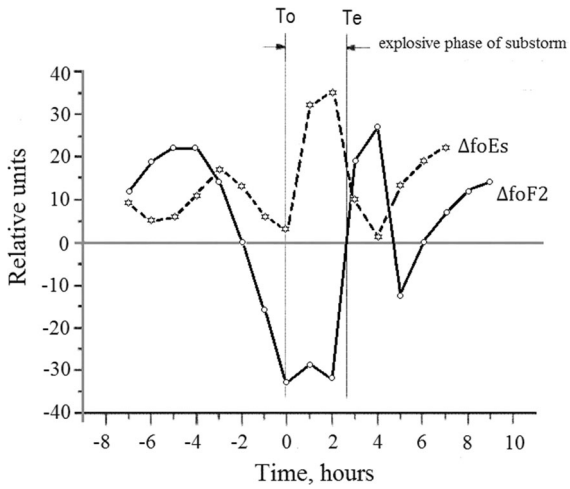

Figure 5
Averaged variations of ΔfoF2 and ΔfoEs during the period of the averaged substorm (taken from Blagoveshchensky et al. 2017)

During the more intense substorm (lower panel) F2MOF grew more significantly than during the weaker substorm up to the full signal absorption at 00:30 UT. This is in accord with Fig. 3. As for the sporadic ionization, it was well-pronounced within the $T_o - T_e$ interval, similarly to the weaker substorm. EsMOF values were higher than F2MOF values within this interval. EsLOF values in this case significantly exceeded the same values during the weaker substorm. This is again due to the higher absorption level.

4.2.3 Averaged Variations

Figure 6 shows the averaged plots of radio propagation parameters F2MOF, F2LOF, EsMOF and EsLOF. Δ is the difference between the values during disturbed and quiet periods, as for example between the values plotted in the upper and middle panels of Fig. 4. These plots are for the weaker substorm because during the intense substorm there were many more gaps in the reflected signal data due to the higher absorption level. The experiment proved that these variations depend more on the location of path reflection point than on its length. A path's length influences the absolute values of MOF and LOF, but not their variations during substorms. In this study the variations are of interest. They depend on the reflection point location during the particular substorm.

All the plotted data obtained at 10 paths were divided in three groups depending on their mid-points location: (1) the three more southern paths with the reflection points at latitudes between 64° N and 66° N; (2) four middle paths with reflection points at latitudes between 68° N and 69.5° N; and (3) the three northern paths with latitudes between 70° N and 72.5° N. Furthermore, the averaging of ΔF2MOF and of ΔEsMOF was performed for each group. The results of this averaging are shown in the three corresponding left panels of Fig. 6. Similarly, averaging was performed for ΔF2LOF and ΔEsLOF during the weaker substorm. The results are shown in the three right panels of Fig. 6.

1. MOF variations.

First, the ΔF2MOF values increase slightly within T_o–T_e from the lower panel to the upper panel, in other words with the latitude increase. Second, the range of increased (more than zero) ΔF2MOF values expands in time with latitude as well. More specifically, the expansion occurs towards the time moments before the substorm beginning. In the lower plot, the beginning of the range with the increased F2MOF values is at 20 UT. In the middle plot it is at 17:40 UT and in the upper plot at 16:40 UT.

The lower panel is characterized by the weak wave-like change of ΔF2MOF values, similar to the Main Effect manifestation shown in Fig. 5 but shifted in time. This effect exists for the southern paths but is masked with the ionization provoked by the precipitations during the substorm.

As for the increased (more than zero) ΔEsMOF, its behavior in the lower plot has common features with the mid-latitude behavior shown in Fig. 5. At high latitudes in upper panels this similarity is absent. There is a tendency for ΔEsMOF appearance before the beginning of the substorm: the higher the latitude, the earlier sporadic formations appear. The earlier occurrence of ΔFMOF and ΔEsMOF with higher latitudes is probably because the northern paths' reflection points are in the auroral oval, and southern path (lower panel) in the subauroral zone.

It is known that during substorms, intense particle fluxes are typically observed; they are less intense

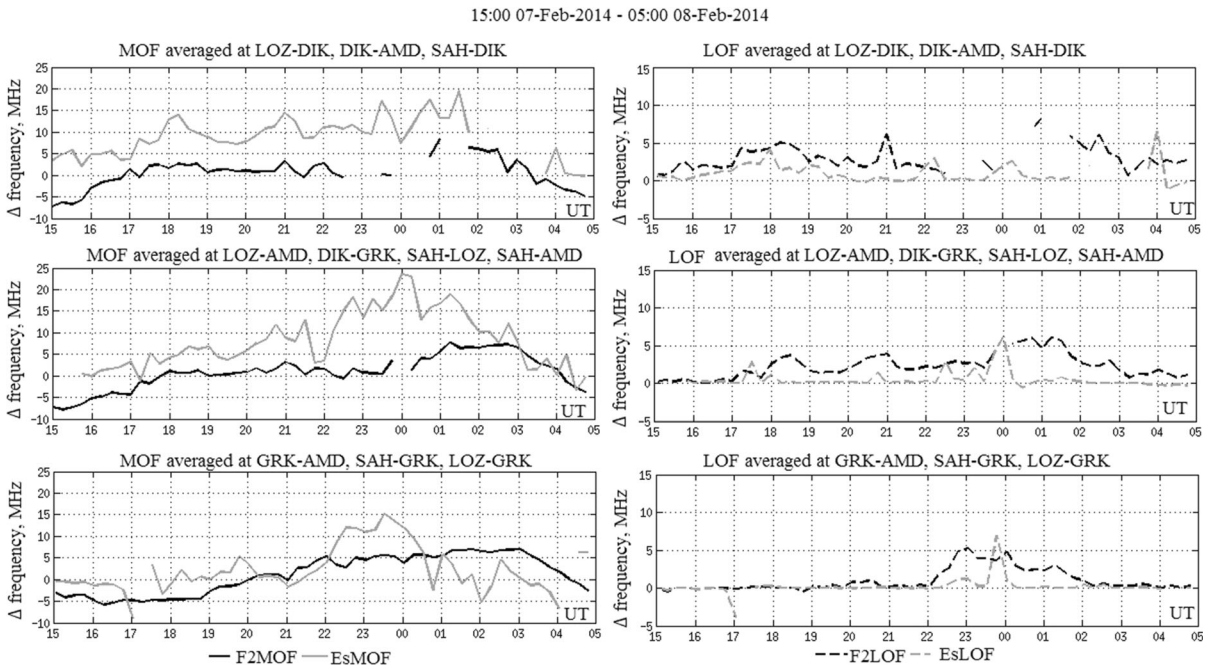

Figure 6
Variations of MOF (left panels) and LOF (left panels) during the weaker substorm averaged at more northern paths (upper panels), middle paths (middle panels) and the more southern paths (lower panel)

south of the oval (Hunsucker and Hargreaves 2003). The more intense the fluxes, the more intense the ionization of the ionosphere. Thus, the considered regularities of ΔF2MOF and ΔEsMOF behavior at high latitudes even during the weak substorm significantly differ from the same regularities at middle latitudes (Fig. 5).

The impact of the more intense substorm on ΔF2MOF and ΔEsMOF in general repeats the regularities of their variations during the weaker substorm (thus not shown in Fig. 6) but with some differences. The smoothing of the Main Effect during the intense substorm for ΔF2MOF is more pronounced because of the intense particle precipitations within T_o-T_e. As for ΔEsMOF, their amplitude before T_o is higher than during the weaker substorm. This is again due to more intense particle precipitations.

2. LOF variations.

Let us consider ΔF2LOF and ΔEsLOF during the weaker substorm. LOF of the F2 layer is known to be an indicator of the absorption level at a path. The higher F2LOF, the higher the absorption level. Regarding EsLOF, the same statement is not obvious and needs additional study. According to Fig. 3, the increased absorption level at paths could be expected during the disturbed conditions between 22 and 0:30 UT of February 7–8, 2014 (T_o-T_e). Indeed, the plots confirm the growth of ΔF2LOF within T_o-T_e and thus the absorption increase. The higher latitudes showed the more increased absorption level. There are almost no ΔF2LOF data from 22:30 UT due to the complete absorption at the higher latitudes (upper plot). Physically, this is explained by the fact that statistically the absorption level (by riometer data) in the center of the oval is higher than at its edges. ΔEsLOF showed some tendency to increase in the form of the drastic bursts within T_o-T_e, with the maximal bursts between 23:30 and 0:30 UT during the peak riometer absorption according to Fig. 3. However, no other clear regularities are seen here.

5. Conclusions

The available oblique sounding data from all high-latitude paths/stations during both disturbance and related quiet (for comparison) periods are very limited. Therefore, every case study is important to improve our understanding of the radio propagation conditions in the Arctic. We addressed the effects of two substorms with a twofold difference in intensity. Data from 10 unique oblique sounding paths were used for the analysis. This case study illustrates the substorm intensity impact on the signal propagation under otherwise similar conditions. New features of radio propagation at high-latitude oblique paths were revealed.

1. A path length influences the absolute MOF and LOF values, but not their variations during substorms. The variations of propagation parameters (ΔMOF and ΔLOF) depend more on the path reflection point location and on the intensity of a substorm. This result is new.
2. The absorption of signals was more pronounced during the more intense substorm which resulted in a loss of information during the transmissions through HF channels.
3. ΔF2MOF variations corresponded to the Main Effect pattern during both substorms, but were shifted in time during the more intense substorm.

It was found that two substorms with a twofold difference in intensity had rather similar effects on ΔMOF, except for (a) the more pronounced smoothing of the Main Effect and (b) the higher ΔEsMOF amplitude during the intense substorm. Both issues are explained by more intense particle precipitations during the more intense disturbance. This result is new.

4. The following features were also revealed
   (a) The results of comparison of two paths of the same length and orientation (with the reflection point in the auroral oval and with the reflection point at the southern edge of the oval) showed that MOF values at the more northern path were higher under both quiet and weakly disturbed conditions because of the higher ionization rate in the center of the oval than at its edges.
   (b) ΔF2MOF increased slightly with latitude during the expansion phase (from data for 10 paths). The range of the ΔF2MOF>0 expanded with latitude towards the moments before the substorm beginning. The earlier ΔF2MOF and ΔEsMOF appearance at higher latitudes is probably because the more northern paths have reflection points in the auroral oval and more southern paths in the subauroal zone.
   (c) F2LOF is known to be higher with a higher absorption level, which has been proved by observations. The higher-latitude paths showed complete absorption, which is explained by the fact that statistically, by riometer data, the absorption level in the centre of the oval is higher than at its edges. No obvious tendency was revealed for EsLOF.

Acknowledgements

This work was supported by Grant no. 18-05-00343 from the Russian Foundation for Basic Research. LANCE acknowledges partial support from CONACyT LN-299022, CONACyT PN 2015-173 and CONACyT-AEM Grant 2017-01-292684. The authors would like to thank the services of Sodankyla Geophysical Observatory, Finland, for providing data and the opportunity of using some data via the Internet (www.sgo.fi) and the Department of Geophysics of Arctic and Antarctic Research Institute, Russia (www.geophys.aari.ru) for the provided OIS ionosonde data as well as magnetometer and riometer data. The OMNI data (geomagnetic indices) were obtained from the GSFC/SPDF OMNIWeb interface at https://omniweb.gsfc.nasa.gov.

References

Angling, M., Cannon, P. S., Davies, N. C., & Arthur, P. S. (1997). Estimation of the availability of data modems on oblique high latitude HF paths. *IEEE Publications*. https://doi.org/10.1049/cp:19970781.

Athiento, R., & Jayachandran, P. T. (2016). MUF variability in the Arctic region: A statistical comparison with the ITU-R variability factors. *Radio Science, 51*, 1278–1285. https://doi.org/10.1002/2016RS006096.

Blagoveshchenskii, D. V. (2013). Effect of magnetic storms (Substorms) on HF propagation: A review. *Geomagnetism and Aeronomy, 53*(4), 409–423. https://doi.org/10.1134/S0016793213040038.

Blagoveshchensky, D. V. (2012). *Space weather and ionospheric radio waves*. Saarbrücken: Palmarium Academic Publishing.

Blagoveshchenskii, D. V. (2016). Anomalous phenomena on HF radio paths during geomagnetic disturbances. *Geomagnetism and Aeronomy, 56*(4), 448–456. https://doi.org/10.1134/S0016793216040022.

Blagoveshchensky, D. V., Kalishin, A. S., & MacDougall, J. (2009). Effects of a "day-time" substorm on the ionosphere and radio propagation. *Advances in Space Research, 44*(9), 1008–1012. https://doi.org/10.1016/j.asr.2009.06.019.

Blagoveshchensky, D. V., Sergeeva, M. A., & Kozlovsky, A. (2017). Ionospheric parameters as the precursors of disturbed geomagnetic conditions. *Advances in Space Research, 60*(11), 2437–2451. https://doi.org/10.1016/j.asr.2017.09.013.

Blagoveshchensky, D. V., Vystavnoi, V. M., & Sergeeva, M. A. (2005). HF radio propagation through the auroral oval during substorms. *Journal of Atmospheric And Solar-Terrestrial Physics, 67*(16), 1618–1625. https://doi.org/10.1016/j.jastp.2005.08.022.

Clilverd, M. A., Rodger, C. J., Brundell, J., Bahr, J., Cobbett, N., Moffat-Griffin, T., et al. (2008). Energetic electron precipitation during substorm injection events: High-latitude fluxes and an unexpected midlatitude signature. *Journal of Geophysical Research-Space Physics*. https://doi.org/10.1029/2008JA013220.

Danilov, A. D., & Konstantinova, A. V. (2019a). Behavior of the ionospheric F region prior to geomagnetic storms. *Advances in Space Research, 64*(7), 1375–1387. https://doi.org/10.1016/j.asr.2019.07.014.

Danilov, A. D., & Konstantinova, A. V. (2019b). Ionospheric precursors of geomagnetic storms, 1. A review of the problem. *Geomagnetism and Aeronomy, 59*(5), 554–566. https://doi.org/10.1134/S0016793219050025.

Durgonics, T., Komjathy, A., Verkhoglyadova, O., Shume, E. B., Benzon, H.-H., Mannucci, A. J., et al. (2017). Multiinstrument observations of a geomagnetic storm and its effects on the Arctic ionosphere: A case study of the 19 February 2014 storm. *Radio Science, 52*, 146–165. https://doi.org/10.1002/2016RS006106.

Hunsucker, R. D., & Hargreaves, J. K. (2003). *The high-latitude ionosphere and its effects on radio propagation* (pp. 477–482). Cambridge: Cambridge University Press.

Karpachev, A. T. (2019). Model of the ionospheric trough for daytime winter conditions based on data from interkosmos-19 and Champ Satellites. *Geomagnetism and Aeronomy, 59*(4), 383–397. https://doi.org/10.1134/S0016793219040091.

Kotova, D. S., Klimenko, M. V., Klimenko, V. V., & Zakharov, V. E. (2017). Influence of geomagnetic storms of September 26–30, 2011, on the Ionosphere and HF Radiowave Propagation II. Radiowave Propagation. *Geomagnetism and Aeronomy, 57*(3), 288–300. https://doi.org/10.1134/S0016793217030100.

Kotova, D. S., Klimenko, M. V., Klimenko, V. V., & Zakharov, V. E. (2015). Numerical simulation of the influence of the May 2–3, 2010. *Radiophysics and Quantum Electronics, 57*, 7. https://doi.org/10.1007/s11141-014-9529-2.

Kotova, D., Ovodenko, V., Yasyukevich, Yu, Klimeno, M., Ratovsky, K., Mylnikova, A., et al. (2020). Efficiency of updating the ionospheric models using total electron content at mid- and sub-auroral latitudes. *GPS Solutions*. https://doi.org/10.1007/s10291-019-0936-x.

Maltseva, O. A., & Mozhaeva, N. S. (2017). Features of behaviour of parameters of the ionosphere of high latitudes in moderate solar activity. *IEEE Publications*. https://doi.org/10.1109/RSEMW.2017.8103584.

Milan, S. E., Jones, T. B., Lester, M., Warrington, E. M., & Reeves, G. D. (1996). Substorm correlated absorption on a 3200 km trans-auroral HF propagation path. *Annales Geophysicae, 14*(2), 182–190.

Milan, S., Jones, T. B., Warrington, M., & Reeves, G. D. (1994). Observations of substorm associated absorption events on a 3200 km high latitude HF propagation path. *IEEE Publications*. https://doi.org/10.1049/cp:19940467.

Parkinson, M. L., Chisham, G., Pinnock, M., Dyson, P. L., & Devlin, J. C. (2004). Magnetic local time, substorm, and particle precipitation-related variations in the behaviour of SuperDARN Doppler spectral widths. *Annales Geophysicae, 22*(12), 4103–4122. https://doi.org/10.5194/angeo-22-4103-2004.

Rogers, N. C., & Honary, F. (2015). Assimilation of real-time riometer measurements into models of 30 MHz polar cap absorption. *Journal of Space Weather and Space Climate, 5*, A8.

Ritchie, S. E., & Honary, F. (2009). Storm sudden commencement and its effect on high-latitude HF communication links. *Space Weather, 2009*(7), S06005. https://doi.org/10.1029/2008SW000461.

Sreeja, V., & Aquino, M. (2014). Statistics of ionospheric scintillation occurrence over European high latitudes. *Journal of Atmospheric and Solar-Terrestrial Physics, 120*, 96–101. https://doi.org/10.1016/j.jastp.2014.09.003.

Siddle, D. R., Stocker, A. J., Warrington, E. M., Zaalov, N. Y., & Homam, M. J. (2013). Simultaneous observations of transionospheric and HF ionospheric propagation within the polar cap. *Radio Science, 48*, 564–572. https://doi.org/10.1002/rds.20062.

Themens, D. R., Jayachandran, P. T., Galkin, I., & Hall, C. (2017). The Empirical Canadian High Arctic Ionospheric Model (E-CHAIM): NmF2 and hmF2. *Journal of Geophysical Research Space Physics, 122*, 9015–9031. https://doi.org/10.1002/2017JA024398.

Uryadov, V. P., Vertogradov, G. G., & Vertogradova, E. G. (2012). Influence of an inhomogeneous structure of the high-latitude ionosphere on the long-distance propagation of high-frequency radio waves. *Radiophysics and Quantum Electronics, 55*(4), 232–240.

Uryadov, V. P., Kolchev, A. A., Vertogradov, G. G., Vybornov, F. I., Egoshin, I. A., Sklyarevsky, M. S., et al. (2017). Impact of a strong magnetic storm and two x-ray flares on the ionospheric HF channel in the summer solstice of 2015 according to oblique sounding in the Eurasian region. *Radiophysics and Quantum Electronics, 60*, 5. https://doi.org/10.1007/s11141-017-9806-y.

Witvliet, B. A., & Alsina-Pagès, R. M. (2017). Radio communication via Near Vertical Incidence Skywave propagation: An overview. *Telecommunication System, 66*, 295–309. https://doi.org/10.1007/s11235-017-0287-2.

(Received December 22, 2019, revised May 5, 2020, accepted June 18, 2020, Published online September 8, 2020)